Supporting Information

A Highly Sensitive Ratiometric Near-Infrared Nanosensor based on Erbium-Hyperdoped Silicon Quantum Dots for Iron(III) Detection

Kun Wang[1], Wenxuan Lai[1], Zhenyi Ni[1, *], Deren Yang[1, 2], and Xiaodong Pi[1, 2, *]

[1]State Key Laboratory of Silicon and Advanced Semiconductor Materials & School of Materials Science and Engineering, Zhejiang University, Hangzhou, Zhejiang 310027, China

[2]Institute of Advanced Semiconductors & Zhejiang Provincial Key Laboratory of Power Semiconductor Materials and Devices, ZJU-Hangzhou Global Scientific and Technological Innovation Center, Zhejiang University, Hangzhou, Zhejiang 311215, China

E-mail: xdpi@zju.edu.cn, zyni@zju.edu.cn

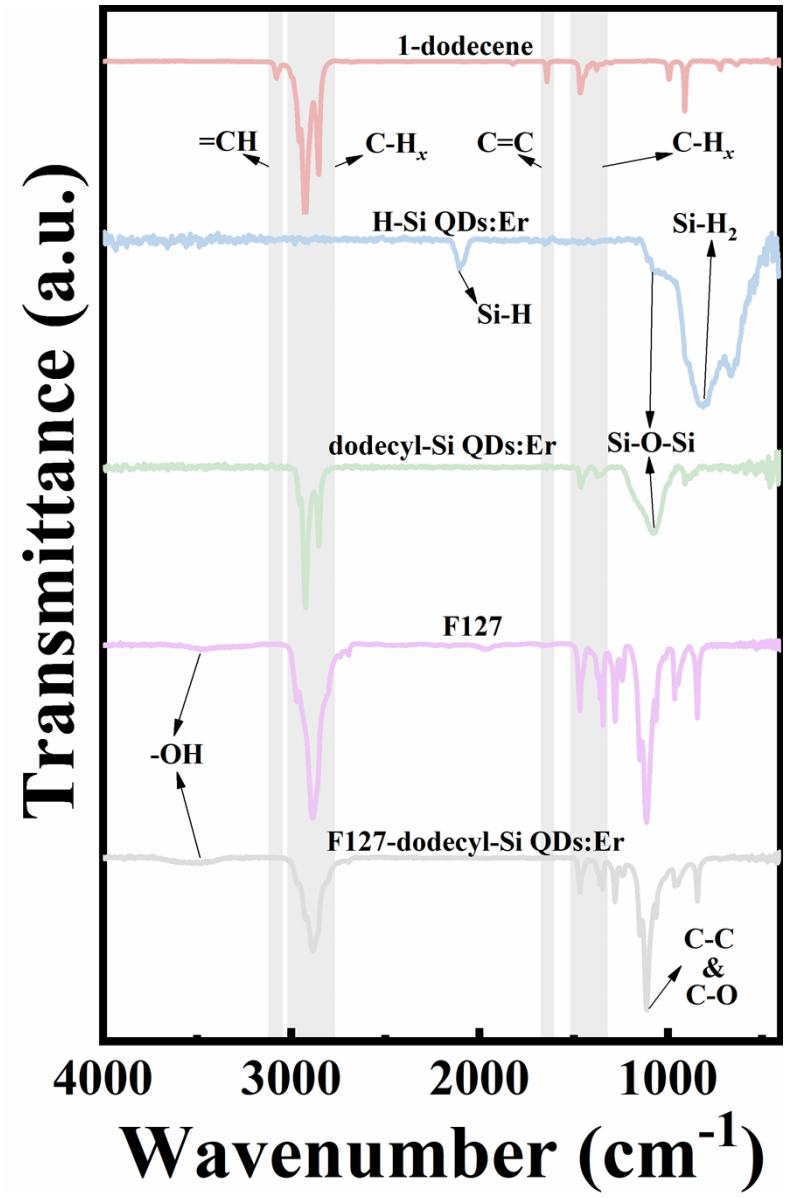

Fig. S1. FTIR spectra of 1-dodecene, Er-hyoerdoped Si QDs after HF etching (H-Si QDs:Er), dodecyl-passivated Er-hyperdoped Si QDs (dodecyl-Si QDs:Er), F127, and dodecyl-passivated Er-hyperdoped Si QDs encapsulated in the micelles using F127 (F127-dodecyl-Si QDs:Er).

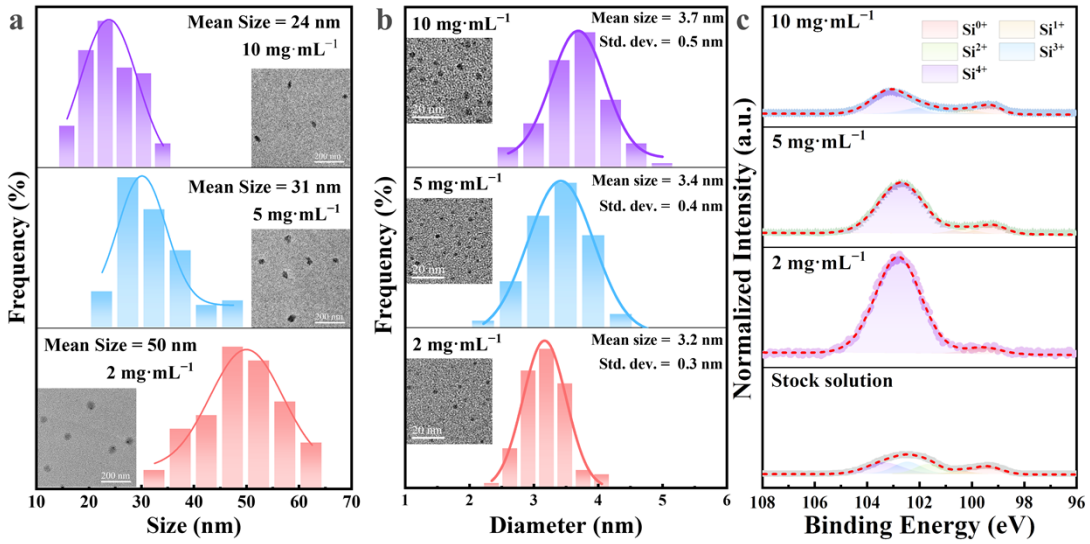

Fig. S2. (a) F127 concentration dependence of F127-dodecyl-Si QDs:Er micelle size distribution. TEM images are shown as the inset. (b) F127 concentration dependence of Si QD size distribution within micelles. TEM images are shown as the inset. (c) Si 2p XPS spectra of stock solution (dodecyl-Si QDs:Er in toluene) and water solution of F127-dodecyl-Si QDs:Er. The concentration of F127 used for the preparation of F127-dodecyl-Si QDs:Er varies from 2 to 10 mg·mL^{-1}.

Table S1. Atomic fraction of various charge states of Si obtained by analyzing the XPS data for dodecyl-Si QDs:Er and F127-dodecyl-Si QDs:Er.

F127 (mg·mL^{-1})	**N_{Si}^{0}**	**N_{Si}^{1+}**	**N_{Si}^{2+}**	**N_{Si}^{3+}**	**N_{Si}^{4+}**	**d (nm)**
Stock solution	17.51%	4.56%	19.71%	25.89%	32.33%	1.07
2	4.95%	0.00%	0.00%	0.00%	95.05%	1.43
5	9.16%	4.59%	0.00%	0.00%	86.24%	1.29
10	13.31%	8.27%	0.00%	18.44%	59.99%	1.18

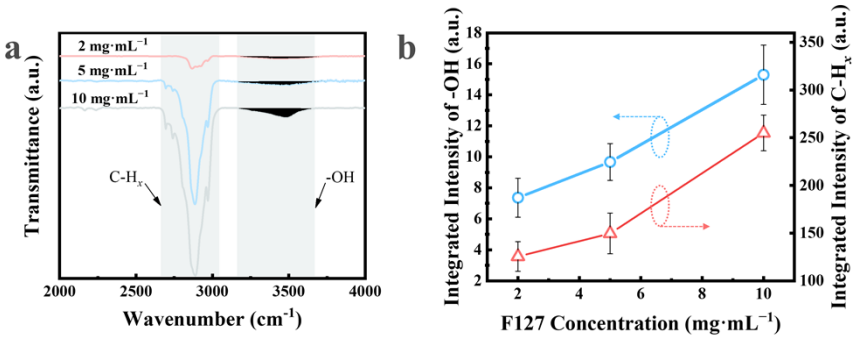

Fig. S3. (a) FTIR spectra of F127-dodecyl-Si QDs:Er assembled from different F127 concentration. (b) Dependence of integrated intensity of -OH and C-H_x on F127 concentration.

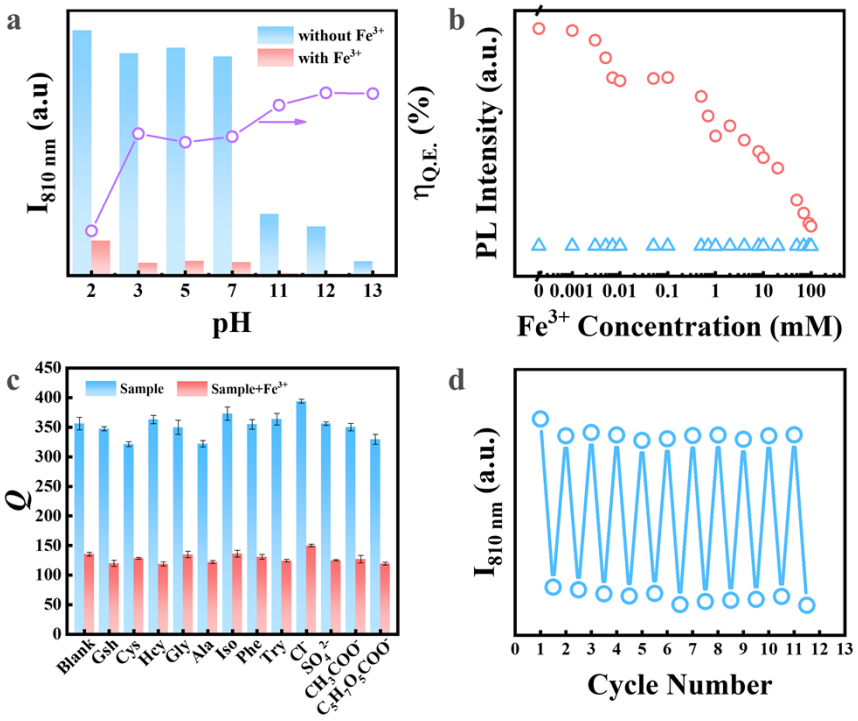

Fig. S4. (a) Effect of pH on PL intensity of F127-dodecyl-Si QDs:Er at 810 nm in the presence of Fe^{3+}. C_{Fe} = 5 mM. (b) Fe^{3+} concentration-dependent integrated PL intensities of Si QDs (810 nm) and Er^{3+} (1540 nm). (c) Selectivity and anti-interference testing of the F127-dodecyl-Si QDs:Er nanosensor against common biological analytes , including biothiols (glutathione (Gsh), cysteine (Cys), homocysteine (Hcy)), amino acids (glycine (Gly), alanine (Ala), isoleucine (Iso), phenylalanine (Phe), tryptophan (Try)), and biological anions (Cl^-, SO_4^{2-}, CH_3COO^-, $C_5H_7O_5COO^-$). All metal ions present are at a concentration of 5 mM. (d) The fluorescence change of F127-dodecyl-Si QDs:Er at 810 nm with the cycle number increasing.

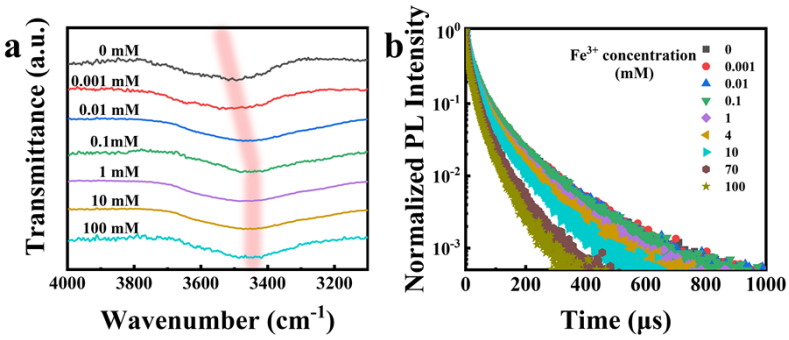

Fig. S5. (a) FTIR spectra of F127-dodecyl-Si QD:Er under different Fe^{3+} concentration. The transparent red line is drawn to guide the eye. (b) PL decay curves of F127-dodecyl-Si QDs:Er under different Fe^{3+} concentration. The emission wavelength (λ_{em}) is 810 nm.

Table S2. Comparison of detection performance metrics to previously reported QDs-based Fe^{3+} nanosensors.

Year	Materials	Dual Emission (nm)	LOD (μM)	Linear range (μM)	VIS/NIR*	Ref.
2014	Graphene QDs	360, 425	0.3	1 – 40	VIS	[1]
2018	CdTe QDs	445, 633	1.5	80 – 1600	VIS	[2]
2019	Carbon QDs	470, 655	0.8	2.5 – 30	VIS	[3]
2019	CdTe QDs	553, 635	0.026	0 – 3.25	VIS	[4]
2019	BSA-Au/Ag QDs	485, 660	1.11	5 – 1000	VIS	[5]
2020	Carbon QDs	416, 688	0.083	0.1 – 40	VIS	[6]
2020	Carbon QDs	458, 612	0.897	0 – 6	VIS	[7]
2020	Carbon QDs	470, 570	0.8	0 – 50	VIS	[8]
2020	Carbon QDs	330, 640	3.75	2 – 27	VIS	[9]
2021	Carbon QDs	321, 382	0.47	2 – 360	VIS	[10]
2022	CdSe/ZnS@SiO2 QDs	425, 530	0.04	0 – 1	VIS	[11]
2022	Carbon QDs	490, 570	0.03	0 – 5	VIS	[12]
2024	**Er-Si QDs**	**810, 1540**	**0.06**	**0 – 10 and 10000 – 100000**	**NIR**	**This work**

* VIS: 380 – 700 nm[13]; NIR: 700 – 2500 nm[14]

Reference

[1] Qu Z bei, Zhang M, Zhou T, et al. A single-wavelength-emitting ratiometric probe based on phototriggered fluorescence switching of graphene quantum dots. Chemistry, 2014, 20, 13777

[2] Zhou M, Guo J, Yang C. Ratiometric fluorescence sensor for Fe^{3+} ions detection based on quantum dot-doped hydrogel optical fiber. Sensors Actuators, B Chem, 2018, 264, 52

[3] Wang Y, Lao S, Ding W, et al. A novel ratiometric fluorescent probe for detection of iron ions and zinc ions based on dual-emission carbon dots. Sensors Actuators, B Chem, 2019, 284, 186

[4] Kuang Y, Wang X, Tian X, et al. Silica-embedded CdTe quantum dots functionalized with rhodamine derivative for instant visual detection of ferric ions in aqueous media. J Photochem Photobiol A Chem, 2019, 372, 140

[5] Li J, Qiao D, Zhao J, et al. Ratiometric fluorescence detection of Hg^{2+} and Fe $^{3+}$ based on BSA-protected Au/Ag nanoclusters and His-stabilized Au nanoclusters. Methods Appl Fluoresc, 2019, 7, 045001

[6] Chen Z, Xu X, Meng D, et al. Dual-emitting N/S-doped carbon dots-based ratiometric fluorescent and light scattering sensor for high precision detection of Fe(III) ions. J Fluoresc, 2020, 30, 1007

[7] Guo X, Pan Q, Song X, et al. Embedding carbon dots in Eu^{3+}-doped metal-organic framework for label-free ratiometric fluorescence detection of Fe^{3+} ions. J Am Ceram Soc, 2021, 104, 886

[8] Pang S, Liu S. Dual-emission carbon dots for ratiometric detection of Fe^{3+} ions and acid phosphatase. Anal Chim Acta, 2020, 1105, 155

[9] Liu Q, Zhao F, Shi B, et al. Mussel-inspired polydopamine-encapsulated carbon dots with dual emission for detection of 4-nitrophenol and Fe^{3+}. Luminescence, 2021, 36, 431

[10] Wang B, Zhou X Q, Lin J M, et al. Concentration-modulated dual-excitation fluorescence of carbon dots used for ratiometric sensing of Fe^{3+}. Microchem J, 2021, 164, 106028

[11] Liu Y, Hu X, Liang F, et al. A FRET sensor based on quantum dots–porphyrin assembly for Fe(III) detection with ultra-sensitivity and accuracy. Anal Bioanal Chem, 2022, 414, 7741

[12] Nandi N, Choudhury K, Sarkar P, et al. Ratiometric multimode detection of pH and Fe^{3+} by dual-emissive heteroatom-doped carbon dots for living cell applications. ACS Appl Nano Mater, 2022, 5, 17315

[13] Kim M, Chen C, Yaari Z, et al. Nanosensor-based monitoring of autophagy-associated lysosomal acidification in vivo. Nat Chem Biol, 2023, 19, 1448

[14] Go M, Hong I, Lee D, et al. Ultrabroadband absorptive refractory plasmonics for

photocatalytic hydrogen evolution reactions. NPG Asia Mater, 2024, 16, 4